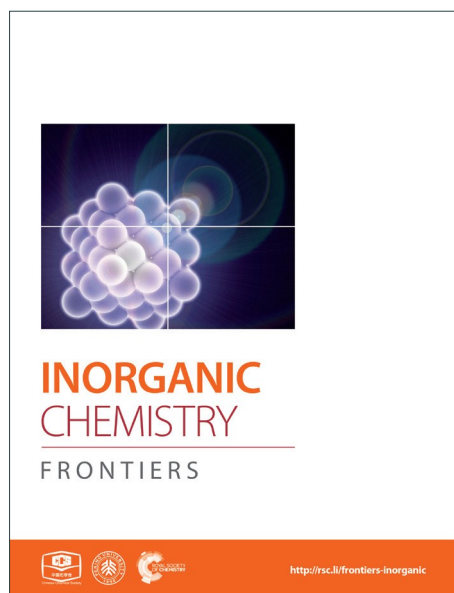
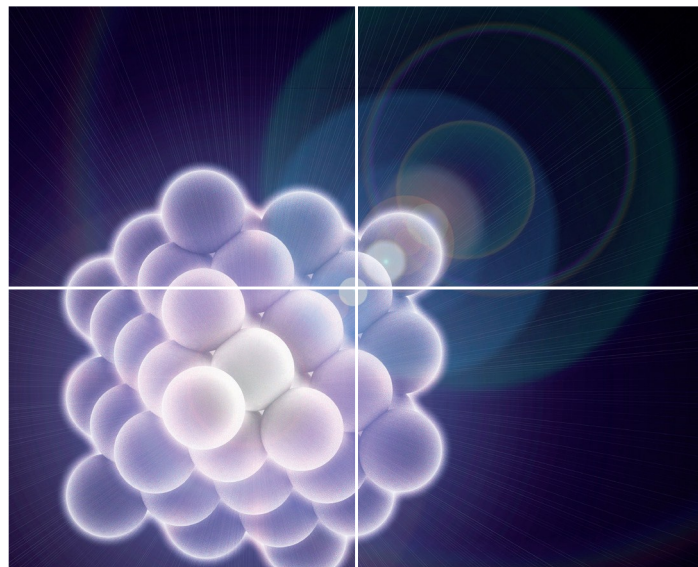


# INORGANIC CHEMISTRY

FRONTIERS

Accepted Manuscript



This is an *Accepted Manuscript*, which has been through the Royal Society of Chemistry peer review process and has been accepted for publication.

*Accepted Manuscripts* are published online shortly after acceptance, before technical editing, formatting and proof reading. Using this free service, authors can make their results available to the community, in citable form, before we publish the edited article. We will replace this *Accepted Manuscript* with the edited and formatted *Advance Article* as soon as it is available.

You can find more information about *Accepted Manuscripts* in the [Information for Authors](#).

Please note that technical editing may introduce minor changes to the text and/or graphics, which may alter content. The journal's standard [Terms & Conditions](#) and the [Ethical guidelines](#) still apply. In no event shall the Royal Society of Chemistry be held responsible for any errors or omissions in this *Accepted Manuscript* or any consequences arising from the use of any information it contains.



(Revised)

## Dispersion and Distribution of Bimetallic Oxides in SBA-15, Its Enhanced Activity for Reverse Water Gas Shift Reaction

Received 00th January 20xx,  
Accepted 00th January 20xx

DOI: 10.1039/x0xx00000x

www.rsc.org/

Baowang Lu,<sup>a</sup> Yiwen Ju,<sup>b</sup> Takayuki Abe<sup>a</sup> and Katsuya Kawamoto<sup>c</sup>

We used the direct hydrothermal synthesis method to obtain various well-dispersed bimetallic oxides/SBA-15 for the first time. It is possible that well-dispersed relatively large bimetallic sulfates were formed during the hydrothermal synthesis process and then re-dispersed with difficulty during the heat treatment process resulting in the formation of well-dispersed oxide particles in SBA-15. TEM elemental maps of CuO-NiO/SBA-15 clearly illustrated that CuO and NiO particles were monodispersed in SBA-15. TEM-EDX line analysis revealed that NiO particles were well distributed on the SBA-15 surface, and then covered by CuO particles. TEM elemental maps of CuO-CeO<sub>2</sub>/SBA-15 clearly showed that CuO and CeO<sub>2</sub> particles aggregated slightly in SBA-15. TEM-EDX line analysis showed that CeO<sub>2</sub> particles were well distributed on the SBA-15 surface, and then covered by CuO particles. TEM elemental maps of NiO-CeO<sub>2</sub>/SBA-15 clearly illustrated NiO and CeO<sub>2</sub> particles aggregated slightly in SBA-15. TEM-EDX line analysis revealed that NiO particles were largely mixed with CeO<sub>2</sub> on the SBA-15 surface. Therefore, TEM elemental maps can be used to study the dispersion of bimetallic oxides, and TEM-EDX line analysis is very effective for investigating their distribution in SBA-15. Compared with monometallic oxides/SBA-15, the obtained bimetallic oxides/SBA-15 catalysts exhibited excellent efficiency as regards reducing CO<sub>2</sub> to CO by the reverse water-gas shift (RWGS) reaction. Especially, the bimetallic oxides/SBA-15 catalysts could result in the high CO<sub>2</sub> conversion to CO at low temperature.

### 1 Introduction

The behaviour of a catalyst is usually influenced by its interaction with other catalyst components such as a second catalyst metal, which could be a promoter. The second metal influences the first metal through electronic interactions or is involved in the reaction by bonding directly to reactants or intermediates. Therefore, bimetallic catalysts are generally used because of the enhanced activity and selectivity that may be achieved by two metals working synergistically. Often, the interactions between the two metals are complex and largely unknown, and the preparation of bimetallic catalysts offers an excellent opportunity for their investigation. Moreover, the work by Sinfelt et al has generated considerable interest in the formation, structure and further exploitation of the catalytic activity of bimetallic particles.<sup>1-6</sup> The deposition of catalytically active nanoparticles on support materials with high dispersion is an important and effective strategy for the design of catalysts. Ordered mesoporous materials with their intrinsically high surface areas have been well studied for this purpose. Multicomponent supported metal catalysts can be prepared by a number of synthesis methods, each with its own distinct advantages.<sup>7-8</sup> The most commonly used co-impregnation methods involve a support material that has been modified by the

adsorption of metal ion precursors from solution.<sup>9-18</sup> The condensation of these centers upon reduction (e.g., in flowing H<sub>2</sub> at high temperature) yields the desired bimetallic particle catalysts. Another attractive way of synthesizing supported bimetallic catalysts is to use molecular cluster compounds as precursors.<sup>4</sup> However, because the ability to control the size distribution of particles obtained in this way is quite limited, the supported bimetallic nanoparticles typically lack uniformity as regards size and shape, and the nature of the compositional distributions that characterize the sample is often unknown. Therefore, it is a serious technological challenge to design a synthesis approach for preparing supported bimetallic catalysts with a uniform size and distribution.

The direct hydrothermal synthesis method is an effective approach for preparing mono-dispersed metal nanoparticles in SBA-15.<sup>19-23</sup> It has been verified that mono-dispersed metal nanoparticles have enhanced activity and selectivity. However, there has still been no research on the preparation of well-dispersed bimetallic nanoparticles in mesoporous silica by the direct hydrothermal synthesis method. After considering the above options, we first developed a direct hydrothermal synthesis method in a strongly acid medium to prepare well-dispersed bimetallic nanoparticles in SBA-15. We also investigated the compositional distribution, and catalytic property compared with well-dispersed monometallic nanoparticles in SBA-15.

### 2 Experimental

#### 2.1 Synthesis of bimetallic oxides/SBA-15

Block copolymer Pluronic P123 (Aldrich, EO<sub>20</sub>PO<sub>70</sub>EO<sub>20</sub>, M<sub>av</sub> = 5800) was dissolved in 105 g of deionized water, and then 19.83 g of sulfuric acid (H<sub>2</sub>SO<sub>4</sub>, Wako Chemical, Japan, 95.0 wt%) and an

<sup>a</sup>Hydrogen Isotope Research Center, Organization for Promotion of research, University of Toyama, 3190 Gofuku, Toyama, 930-8555, Japan.

E-mail: baowangl@ctg.u-toyama.ac.jp; Tel: +81-76-445-6933

<sup>b</sup>Laboratory of Computational Geodynamics College of Earth Science, University of Chinese Academy of Sciences, Beijing 100049, China.

<sup>c</sup>Graduate School of Environmental and Life Science, Okayama University, 3-1-1 Tushima-naka, Kita-ku, Okayama-shi, Okayama, 700-8530, Japan.

appropriate quantity of nitrate hexahydrate salts, such as nickel (II) nitrate hexahydrate ( $\text{Ni}(\text{NO}_3)_2 \cdot 6\text{H}_2\text{O}$ , Wako Chemical, Japan, 98.0 wt%), copper (II) nitrate trihydrate ( $\text{Cu}(\text{NO}_3)_2 \cdot 3\text{H}_2\text{O}$ , Wako Chemical, Japan, 99.5 wt%), cerium (III) nitrate hexahydrate ( $\text{Ce}(\text{NO}_3)_3 \cdot 6\text{H}_2\text{O}$ , Wako Chemical, Japan, 98.0 wt%) were added at room temperature. The mixture was stirred for 30 minutes, and then 8.52 g of tetraethylorthosilicate ( $\text{Si}(\text{OC}_2\text{H}_5)_4$ , TEOS, Wako Chemical, Japan, 95.0 wt%) was added. The obtained starting mixture was aged at 60 °C until a white precipitate appeared, and then immediately evaporated at 100 °C overnight ( $\approx 14$  h). The resulting solid product was dried at 150 °C for 5 h, and then calcined at 500 °C for 10 h and at 800 °C for 2 h.

## 2.2 Characterization

The X-ray diffraction (XRD) patterns of the solid products were collected by a powder X-ray diffractometer (Bruker AXS D8 Advance) with graphite monochromatized Cu K $\alpha$  radiation at 40 kV and 40 mA. Nitrogen adsorption isotherms at -196 °C were obtained using a conventional volumetric apparatus (Quadrasorb USA). Before the adsorption measurements were made, the powders ( $\approx 0.1$  g) were subjected to a temperature of 300 °C for 5 h in a vacuum. The specific surface area was calculated with the Brunauer-Emmett-Teller (BET) method. The pore size was calculated from the desorption branch of nitrogen adsorption-desorption isotherms by the Barrett-Joyner-Halenda (BJH) method. The pore volume was taken at a single point  $P/P_0 = 0.95$ . The morphology was observed with a scanning electron microscope (SEM, Oxford Instruments). The solid product was observed using a transmission electron microscope (TEM, JEM-2100F) at an electron acceleration of 200 kV. The TEM-EDX analyses were conducted with an electron beam approximately 1 nm in diameter.

## 2.3 Catalytic property

The RWGS reaction was used as a model reaction to study the catalytic property of NiO/SBA-15. Before the RWGS reaction, the catalysts were pre-reduced in situ in an 80 %  $\text{H}_2/\text{N}_2$  stream for 2 h with a total gas flow of 50 ml/min at 900 °C and a heating ramp rate of 100 °C/h. The RWGS reaction was performed at atmospheric pressure in a fixed-bed quartz reactor with a 20-mm inner diameter in an initial temperature range of 400 to 900 °C. A 30-mm-long catalyst between two layers of quartz wool was loaded into the reactor. A thermocouple was inserted directly into the center of the

catalyst bed to measure the actual pre-treatment and reaction

temperatures in situ. The reactor was heated in a furnace (KTF-035N, Koyo Thermo Systems, Co., Ltd.) equipped with a temperature controller. All reactant gases were monitored with a mass flow meter (E-40) and a controller (PE-D20) (HORIBA STEC, Co., Ltd.). The flow of the product was measured with a film flow meter (VP-3, HORIBA STEC, Co., Ltd.) and analyzed with a gas chromatography-thermal conductivity detector (GC-TCD) after the RWGS reaction had become stable. The turnover frequencies (TOFs) were calculated from the rate of  $\text{CO}_2$  conversion divided by the total amount of NiO used.

## 3 Results and discussion

### 3.1 Synthesis and characterization of bimetallic oxides/SBA-15

As described in detail in experimental section, bimetallic oxides/SBA-15 such as CuO-NiO/SBA-15, CuO-CeO<sub>2</sub>/SBA-15, NiO-CeO<sub>2</sub>/SBA-15 were obtained with a direct hydrothermal synthesis method. For comparison, monometallic oxides/SBA-15 used as reference catalysts, such as CuO/SBA-15 and NiO/SBA-15, were also synthesized using a direct hydrothermal synthesis method. The amounts of metallic oxide in bimetallic oxides/SBA-15 and the reference catalyst are shown in Table 1.

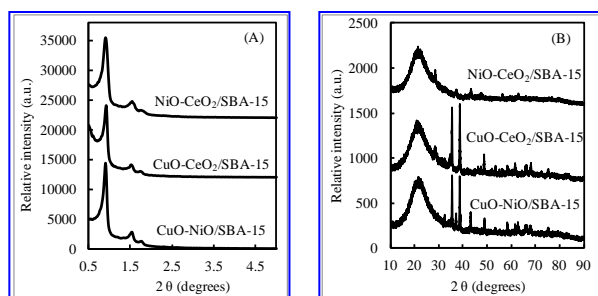
The small-angle XRD patterns (Fig. 1 (A)) of bimetallic oxides/SBA-15 had three well-resolved peaks that could be indexed as (100), (110) and (200) diffraction peaks, indicating the typical two-dimensional hexagonally ordered mesostructure ( $p6mm$ ) of SBA-15.<sup>26,27</sup> In addition, as shown in Fig. 1 (B), the wide-angle XRD peaks could be indexed as various bimetallic oxides. Also, a broad peak at around  $2\theta = 23^\circ$  caused by the amorphous  $\text{SiO}_2$  structure of SBA-15 was clearly observed in the wide-angle XRD patterns, indicating that the ordered mesoporous structure was not disturbed by the incorporation of various bimetallic oxides. The Scherrer equation<sup>28</sup> was used to calculate the average grain size of various bimetallic oxide particles, which is summarized in Table 1. The average size of metallic oxide particles in bimetallic oxides/SBA-15 was larger than that in monometallic oxides/SBA-15, due to the increased amount of metallic oxide in the limited space, indicating metal oxides were not located in the channels of SBA-15 with smaller size, but also on the outside of SBA-15 with larger size. In NiO-CeO<sub>2</sub>/SBA-15, even though the NiO amount was only 1 wt%, the NiO particle size was 21.3 nm, suggesting that the particles were also on the outer SBA-15 surface except in the SBA-15 nano-channels, unlike those in NiO/SBA-15 (only in SBA-15 nano-channels). Therefore, compared with monometallic oxides/SBA-15, both the average size of the metallic oxide particles in bimetallic oxides/SBA-15 became larger,

Table 1 Characteristics, particles grain size and activation energy of various oxides/SBA-15 obtained by direct synthesis method

Metallic oxides /SBA-15	Amount (wt%) <sup>b</sup>	CuO		NiO		CeO <sub>2</sub>		$d_{100}$ (nm)	$S_{\text{BET}}^a$ ( $\text{m}^2\text{g}^{-1}$ )	PV <sup>a</sup> ( $\text{cm}^3\text{g}^{-1}$ )	PS <sup>a</sup> (nm)	WT <sup>a</sup> (nm)	Ea <sup>a</sup> (kcal mol <sup>-1</sup> )		
		GS (nm) <sup>a</sup>	TEM	GS (nm) <sup>a</sup>	TEM	GS (nm) <sup>a</sup>	TEM								
SBA-15	0	-	-	0	-	0	-	10.99	678	1.15	9.15	3.54	-		
CuO/SBA-15	5 (5.02)	29.6	30.1	0	-	0	-	10.06	281	0.90	9.26	2.36	72.8		
CuO-NiO/SBA-15	5 (4.87)	48.1	47.6	1 (0.95)	53.1	0	-	9.80	279	0.82	8.24	3.08	53.6		
CuO/SBA-15	10 (9.89)	36.5	37.1	0	-	0	-	9.79	278	0.85	9.18	2.12	74.7		
CuO-CeO <sub>2</sub> /SBA-15	10 (9.79)	39.4	39.6	0	-	1 (1.02)	13	9.61	194	0.72	8.23	2.87	63.5		
NiO/SBA-15	0	-	-	1 (0.99)	5.2	5.4	0	-	10.86	385	1.10	9.10	3.44	27.8	
NiO-CeO <sub>2</sub> /SBA-15	0	-	-	1 (0.98)	21.3	21.1	1 (1.03)	19.4	19.1	9.78	298	1.03	7.53	3.76	9.5

<sup>a</sup>GS: Grain size calculated by XRD and TEM,  $S_{\text{BET}}$ : Surface area calculated using the Brunauer-Emmett-Teller (BET) method in the relative pressure range of  $p/p_0 = 0.05-0.3$ ; PV: Pore volume obtained from the volumes of  $\text{N}_2$  adsorbed at  $p/p_0 = 0.95$  or in the vicinity; PD: Pore diameter analyzed by the desorption branch of the isotherms using the Barrett-Joyner-Halenda (BJH) method, WT: Wall thicknesses: calculated by  $(2 \times d_{100} / \sqrt{3})$  - pore size, and Ea: activation energy. <sup>b</sup> Value in bracket measured by EDX.

and the distribution was different.



**Fig. 1** Small-angle (A) Wide-angle (B) XRD patterns of various bimetallic catalysts.

Fig. 2 shows the nitrogen adsorption-desorption isotherms of various bimetallic oxides/SBA-15. The isotherms were similar to the type IV IUPAC classification,<sup>29</sup> clearly indicating that these materials had mesoporous structures; a type-H1 hysteresis loop was observed. The isotherm was typical of SBA-15,<sup>26,27</sup> indicating the formation of a *p6mm* structure with open cylindrical mesopores. And there was no blocking effect, unlike that obtained with the post synthesis method.<sup>30,31</sup> This result suggests that NiO particles were dispersed in the SiO<sub>2</sub> structure of SBA-15, not in the SBA-15 pores, in contrast with the post synthesis method.<sup>30,31</sup> Also, one narrow peak was observed in the PSD curve (Fig. 2), showing that a unique pore was present.

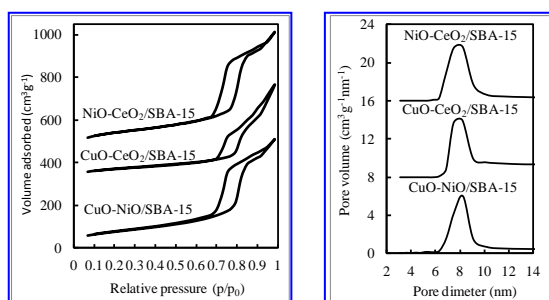


**Fig. 2** Nitrogen adsorption-desorption isotherms and pore size distribution curves of various bimetallic catalysts.

The characteristics of various bimetallic oxides/SBA-15 obtained by the direct hydrothermal synthesis method are summarized in Table 1. Compared with mono-metallic oxides/SBA-15 or SBA-15, the surface area, pore volume and pore size all shrank, indicating that the SBA-15 structure was degraded by the incorporation of bimetallic oxides or mono-metallic oxides. The wall thickness of bimetallic oxides/SBA-15 was thicker than that of monometallic oxides/SBA-15, indicating the reduction of the ordered structure caused by the incorporation of bimetallic oxides.

There have been no reports of the successful synthesis of monodisperse metal particles in strong acid media using conventional HCl to synthesize SBA-15. Using H<sub>2</sub>SO<sub>4</sub> instead of HCl, we successfully obtained monodisperse NiO particles in SBA-15 and reported it for the first time.<sup>25</sup> By dispersing the molten intermediates formed from nitrate during the thermal decomposition process, the oxides can be well dispersed into SBA-15 by heat treatment after mixing the nitrate and SBA-15.<sup>32,33</sup> Therefore, the nitrate and its molten intermediates can move during the heat treatment process, resulting in well-dispersed oxides/SBA-15 with severely agglomerated particles. When using

H<sub>2</sub>SO<sub>4</sub>, the sulphate formed during the hydrothermal synthesis process was relatively larger than nitrate, and so it did not move easily during the heat treatment process, which made it possible to obtain mono disperse metallic oxide particles in SBA-15. H<sub>2</sub>SO<sub>4</sub> was used in this research to obtain various well dispersed bimetallic oxides/SBA-15.

Because nitrate is highly soluble in acid media, bimetallic ions can interact with the hydrophilic ethylene oxide units of Pluronic P123, with the result that metallic ions are likely to be encapsulated within the core of Pluronic P123 micelles. After silica species have polymerized on the surface of Pluronic P123 micelles, the final product contains bimetallic oxides inside the mesoporous framework. However, we cannot exclude the separate formation of SBA-15 with Pluronic P123 and the adsorption of bimetallic oxides on its surface.

Figure 3 shows TEM images and SEM image. The morphology of all bimetallic oxides/SBA-15 consisted of rod-like aggregates; and this was the same as that of typical SBA-15, as previously reported.<sup>26,27,34,35</sup> All bimetallic oxides/SBA-15 had the ordered mesoporous structure of typical SBA-15. Fig. 4 shows TEM elemental maps of various bimetallic oxides/SBA-15. In CuO-NiO/SBA-15, no aggregates of NiO particles were observed clearly, indicating that the CuO and NiO particles were highly dispersed (mono-dispersed) into the SBA-15 structure, unlike in previous reports using the post synthesis method where aggregates were observed.<sup>30,31</sup> However, in CuO-CeO<sub>2</sub>/SBA-15 and NiO-CeO<sub>2</sub>/SBA-15, there was slight but acceptable aggregation of CuO (due to the large amount), CeO<sub>2</sub> (due to its ease of aggregation) and NiO (due to the fact that a small amount disperses into CeO<sub>2</sub>) particles. Therefore, well-dispersed bimetallic oxides/SBA-15 could be obtained by the direct hydrothermal synthesis method. As shown in Table 1, the average size of bimetallic oxides measured by TEM was similar to that calculated by XRD.

We have investigated the distribution of NiO in NiO/SBA-15 obtained by the direct hydrothermal synthesis method.<sup>25</sup> With a small amount of NiO, NiO particles were present in the NiO/SBA-15 pores. As the NiO amount was increased, the NiO particles began to disperse on the outer surface of the NiO/SBA-15. Studying the distribution of bimetallic oxide is very interesting and important.

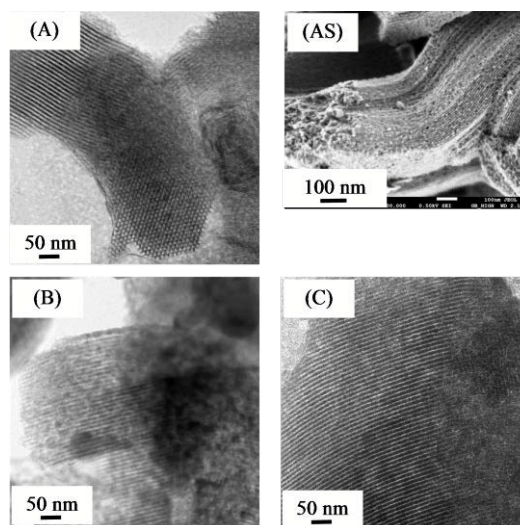


**Fig. 3** TEM images of (A): CuO-NiO/SBA-15, (B): CuO-CeO<sub>2</sub>/SBA-15, (C): NiO-CeO<sub>2</sub>/SBA-15 and SEM image of (AS): CuO-NiO/SBS-15.

Therefore, we investigated the bimetallic oxide distribution using TEM-EDS line profile analysis. The EDS line profiles are shown in Fig. 5. As shown in Table 1, the actual contents of bimetallic oxides obtained by elemental analysis were close to their initial contents in starting synthesis gel. In CuO-NiO/SBA-15 and CuO-CeO<sub>2</sub>/SBA-15, the appearance of the maximum relative atom concentration of every metallic oxide was regular, clearly indicating that every metallic oxide was well dispersed. The position of the maximum relative atom concentration of every metallic oxide appeared in turn, and did not overlap in the same place. The interval distance was about 1 nm, suggesting that one metallic oxide was well distributed on the SBA-15 surface, and then covered by another metallic oxide, and they were not simply mixed together. This phenomenon found for supported bimetallic oxides was very interesting. In CuO-NiO/SBA-15, the distance between the two positions at which the maximum relative atom concentration of every metallic oxide appeared was about 7 to 8 nm, which is close to the pore size of bimetallic oxides/SBA-15 measured by N<sub>2</sub> adsorption. In addition, in NiO-CeO<sub>2</sub>/SBA-15, the positions of the maximum relative atom concentrations of NiO and CeO<sub>2</sub> appeared in almost the same place and overlapped, similar to the bimetallic oxides/SBA-15 prepared by co-impregnation,<sup>36</sup> indicating that the NiO and CeO<sub>2</sub> particles were simply mixed (i.e. NiO was dispersed into CeO<sub>2</sub>), and then dispersed on the SBA-15 surface.

Ni(NO<sub>3</sub>)<sub>2</sub> is hydrophilic relative to Cu(NO<sub>3</sub>)<sub>2</sub> and hydrophobic relative to TEOS. Therefore, TEOS preferentially, and then Ni<sup>2+</sup>

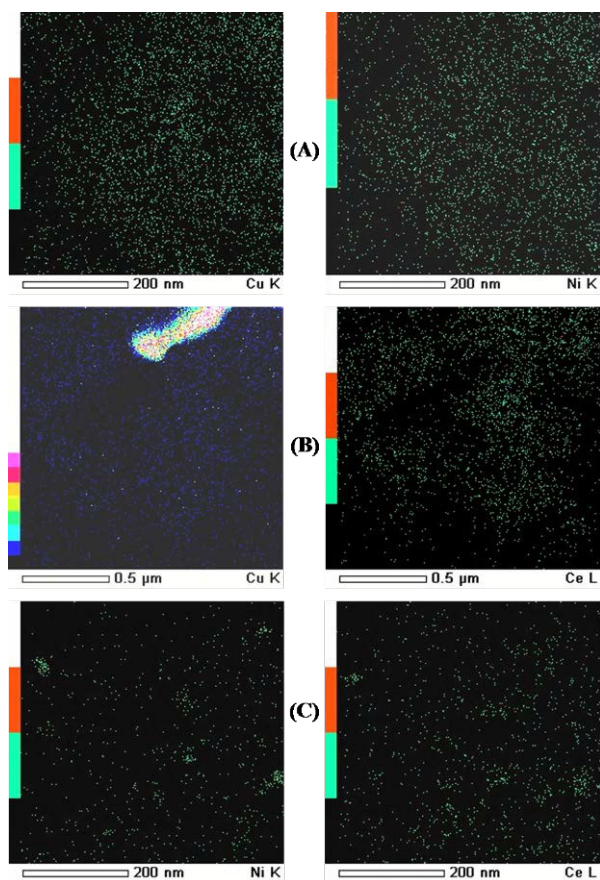


Fig. 4 TEM elemental maps of (A) CuO-NiO/SBA-15, (B) CuO-CeO<sub>2</sub>/SBA-15, (C) NiO-CeO<sub>2</sub>/SBA-15.

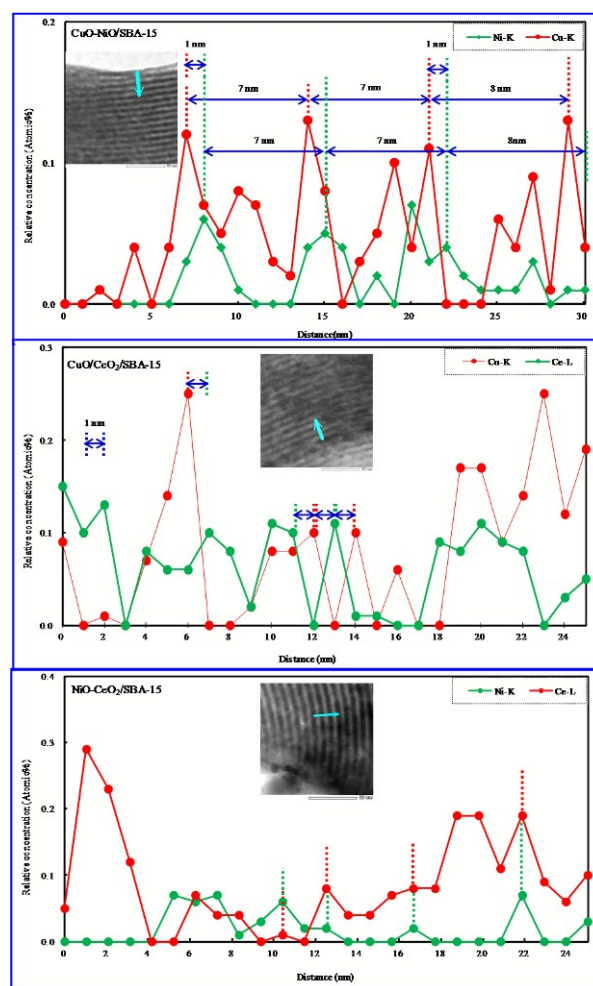


Fig. 5 EDX line profiles of various bimetallic oxides/SBA-15.

followed finally by Cu<sup>2+</sup> interacted with the hydrophilic ethylene oxide units of Pluronic P123, with the result that the NiO particles were covered with CuO particles in CuO-NiO/SBA-15. In the same way, CeO<sub>2</sub> particles were covered by CuO in CuO-CeO<sub>2</sub>/SBA-15. In NiO-CeO<sub>2</sub>/SBA-15, the very few NiO and CeO<sub>2</sub> particles were present as mixtures and they dispersed into the SBA-15 surface. The images of the bimetallic oxide distribution were considered

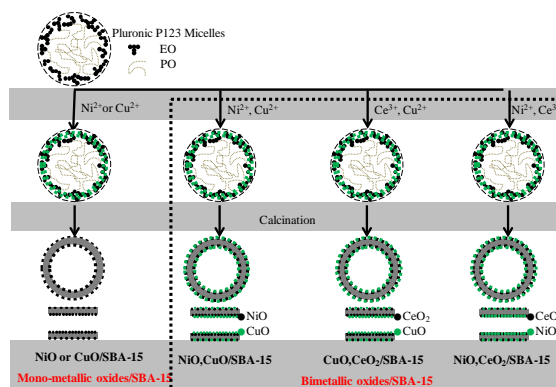


Fig. 6 Distribution images of bimetallic oxides in SBA-15.

based on the above results and shown in Fig.6.

### 3.2 Catalytic property of bimetallic oxides/SBA-15

The conversion of CO<sub>2</sub> to valuable chemical materials has been proposed as a possible way of utilizing greenhouse gas CO<sub>2</sub>.<sup>37-42</sup> In terms of CO<sub>2</sub> conversion, because CO is a valuable material in many chemical processes, the conversion of CO<sub>2</sub> to CO by catalytic hydrogenation is recognized as the most promising process, and the reverse water-gas shift (RWGS) reaction is a highly desirable reaction for CO<sub>2</sub> to CO conversion.<sup>43-56</sup> Therefore, the RWGS reaction was used as a model reaction with which to study the catalytic property of various bimetallic oxides/SBA-15.

To investigate the catalytic property, we attempted to perform the RWGS reaction by fixing the CO<sub>2</sub>/H<sub>2</sub> ratio at 1 using various bimetallic oxides/SBA-15. For comparison, monometallic oxides/SBA-15 was also used to investigate the RWGS reaction. The results are shown in Fig. 7. The CO<sub>2</sub> conversion increased with increasing temperature, suggesting that high temperature favored CO<sub>2</sub> conversion. The CO<sub>2</sub> conversion of all bimetallic oxides/SBA-15 was higher than that of monometallic oxides/SBA-15. Therefore, bimetallic oxides enhanced the activity. Especially, the bimetallic oxides/SBA-15 catalysts could result in the high CO<sub>2</sub> conversion to CO at low temperature due to the presence of the strong interaction between metal (active center) and oxides (promoter), indicating that the RWGS reaction could occur even at low temperature.

The CO<sub>2</sub> conversion of CuO-NiO/SBA-15 was lower than that of NiO/SBA-15, but higher than CuO/SBA-15, indicating that Cu particles maybe play an important role in CO<sub>2</sub> conversion to CO, rather than Ni particles (as promoters), i.e. a large number of NiO particles were covered by CuO particles. This result supported the above EDX line profile analysis. In addition, the large NiO particles formed maybe result lower CO<sub>2</sub> conversion. The CO<sub>2</sub> conversion of CuO-CeO<sub>2</sub>/SBA-15 or NiO-CeO<sub>2</sub>/SBA-15 was higher than that of CuO/SBA-15 or NiO/SBA-15, indicating that a large number of CeO<sub>2</sub> particles were covered by CuO or mixed with NiO particles. This result also supported the above EDX line profile analysis. In this case CeO<sub>2</sub> acted as a promoter, driving force for the CO<sub>2</sub> conversion to CO because of the presence of oxygen vacancies. Therefore, these results supported our above conclusion regarding the distribution of bimetallic oxides in SBA-15.

Figure 8 shows CO selectivity using various bimetallic oxides/SBA-15 and monometallic oxides/SBA-15. Regardless of temperature, all

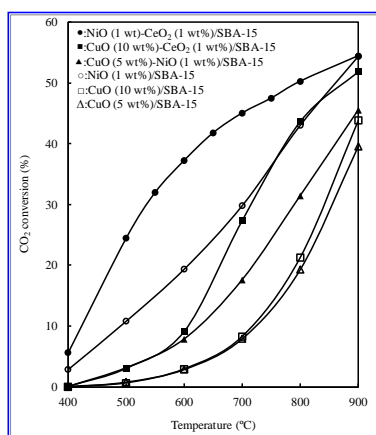


Fig. 7 CO<sub>2</sub> conversion at different temperature with various catalysts obtained by direct synthesis method.

catalysts exhibited a CO selectivity of 100 %, except NiO-CeO<sub>2</sub>/SBA-15. In our previous reports,<sup>25,54</sup> NiO particles were mono-dispersed (isolated) in SBA-15 in the presence of NiO amount of less than 15 wt%, showing a CO selectivity of close to 100 %. Then, Christopher et al. also confirmed that isolated metal active site can exhibit a CO selectivity of close 100 %.<sup>57</sup> However, when NiO-CeO<sub>2</sub>/SBA-15 was used, the CO selectivity was 100 % at high temperature, whereas it was lower than 100 % even at low NiO concentration, due to the formation of methane at low temperature, different from our previous report,<sup>25,54</sup> suggesting that the influence of CeO<sub>2</sub> on CO selectivity should be considered. In our previous research,<sup>55</sup> NiO particles with low concentration were mono-dispersed in CeO<sub>2</sub>, showing a CO selectivity of close to 100 %, while with high concentration those were aggregated in CeO<sub>2</sub>, CO selectivity was lower than 100 %. Therefore, the possibility is that NiO particles in NiO-CeO<sub>2</sub>/SBA-15 were not mono-dispersed.

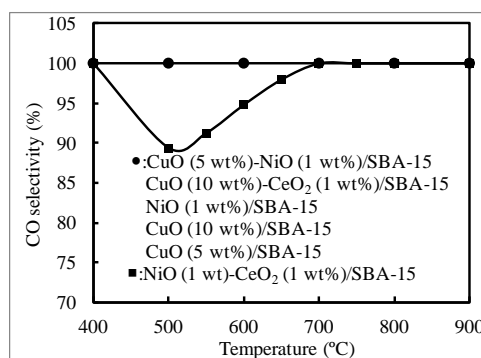


Fig. 8 CO selectivity at different temperature with various catalysts obtained by direct synthesis method.

Figure 9 shows Arrhenius plots for CO<sub>2</sub> conversion using various bimetallic oxides/SBA-15 and monometallic oxides/SBA-15. The activation energy for CO<sub>2</sub> conversion was calculated, and is summarized in Table 1. The difference in activation energy led to their different catalytic activity. The activation energy of various bimetallic oxides/SBA-15 for CO<sub>2</sub> conversion was lower than that of monometallic oxides/SBA-15, suggesting the bimetallic oxides/SBA-15 had enhanced activity due to bimetallic oxide incorporation.

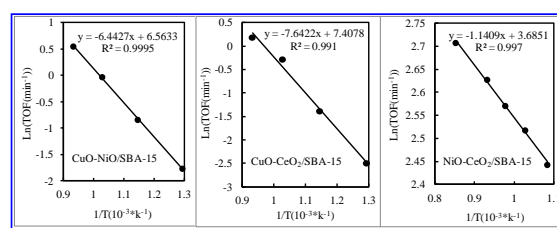


Fig. 9 Arrhenius plots using various bimetallic catalysts obtained by direct synthesis method.

### Conclusions

In summary, by using the direct hydrothermal synthesis method, various bimetallic oxides/SBA-15 were synthesized for the first time. The dispersion and distribution of bimetallic oxides in SBA-15 were investigated by employing TEM elemental maps and TEM-EDX line analysis. The TEM elemental maps showed that various bimetallic

oxides were well dispersed in SBA-15. The TEM-EDX line analysis of CuO-NiO/SBA-15 and CuO-CeO<sub>2</sub>/SBA-15 showed that the first metallic oxide particles were well distributed on the SBA15 surface, and covered by other metallic oxide particles. In NiO-CeO<sub>2</sub>/SBA-15, mixtures of NiO and CeO<sub>2</sub> particles were well distributed on the SBA-15 surface. Compared with monometallic oxides/SBA-15, the obtained bimetallic oxides/SBA-15 catalysts exhibited excellent efficiency. We can expect this direct synthesis method to be used to prepare other bimetallic oxide particles with various supports, and using TEM elemental maps and TEM-EDX line analysis to investigate dispersion and distribution of bimetallic oxides.

## Notes and references

- 1 J. H. Sinfelt, *Bimetallic Catalysts, Concepts, and Applications*, John Wiley & Sons, New York, 1983.
- 2 J. H. Sinfelt, *Int. Rev. Phys. Chem.*, 1988, **7**, 281.
- 3 J. R. Anderson, *Structure of Metallic Catalysts*, Academic Press, New York, 1975.
- 4 K. J. Klabunde and Y. -X. Li, *In Selectivity in Catalysis* (Eds.: M. E. Davis and S. L. Suib), ACS Symposium Series 517, American Chemical Society, Washington, DC, 1993, pp 88-108.
- 5 K. Kinoshita, P. Stonehart, *In Preparation and Characterization of Highly Dispersed Electrocatalytic Materials* (Eds.: K. Kinoshita and P. Stonehart), Plenum, New York, 1977, Vol. **12**, pp 183-266.
- 6 M. Watanabe, M. Uchida, S. Motoo, *J. Electroanal. Chem.*, 1987, **229**, 395.
- 7 O. S. Alexeev and B. C. Gates, *Ind. Eng. Chem. Res.*, 2003, **42**, 1571.
- 8 B. C. Gates, *Chem. Rev.*, 1995, **95**, 511.
- 9 J. Panpranot, J. G. Goodwin and Jr., A. Sayari, *J. Catal.*, 2002, **211**, 530.
- 10 R. Raja, T. Khimiyak, J. M. Thomas, S. Hermans and B. F. G. Johnson, *J. Catal.*, 2003, **213**, 78.
- 11 S. N. Pronkin, P. A. Simonov, V. I. Zaikovskii and E. R. Savinova, *J. Mol. Catal. A: Chem.*, 2007, **265**, 141.
- 12 S. S. Itkulova, K. Z. Zhunusova and G. D. Zakumbaeva, *World*, 2008, **52**, 850.
- 13 M. Dhakada, D. Finob, S. S. Rayalua, R. Kumara, A. Watanabec, H. Hanedac, S. Devotaa, T. Mitsuhashic and N. Labhsetwara, *Topics Catal.*, 2007, **42-43**, 273.
- 14 A. Kulkarni and B. C. Gates, *Angew. Chem. Int. Ed.*, 2009, **48**, 9697.
- 15 C. Montesdecorrea and F. Cordobacastrillon, *J. Mol. Catal. A: Chem.*, 2005, **228**, 267.
- 16 M. S. Nashner, A. I. Frenkel, D. L. Adler, J. R. Shapley and R. G. Nuzzo, *J. Am. Chem. Soc.*, 1997, **119**, 7760.
- 17 B. F. G. Johnson, J. M. Thomas, G. Sankar, D. Ozkaya, W. -Z. Zhou, R. D. Oldroyd and R. G. Bel, *Angew. Chem. Int. Ed. Engi.*, 1997, **36**, 2242.
- 18 P. Doggali, Y. Teraoka, P. Mungse, I. K. Shah, S. Rayalu and N. Labhsetwar, *J. Mol. Catal. A: Chem.*, 2012, **358**, 23.
- 19 W. -Z. Zhou, J. M. Thomas, D. S. Shephard, B. F. G. Johnson, D. Ozkaya, T. Maschmeyer, R. G. Bell and Q. F. Ge, *Science*, 1998, **280**, 705.
- 20 R. Raja, T. Khimiyak, J. M. Thomas, S. Hermans and B. F. G. Johnson, *Angew. Chem. Int. Ed.*, 2001, **40**, 4638.
- 21 D. S. Shephard, T. Maschmeyer, G. Sankar, J. M. Thomas, D. Ozkaya, B. F. G. Johnson, R. Raja, R. D. Oldroyd and R. G. Bell, *Chem. Eur. J.*, 1998, **4**, 1214.
- 22 M. Conte, A. F. Carley, G. A. Attard, A. A. Herzing, C. J. Kiely and G. J. Hutchings, *J. Catal.*, 2008, **257**, 190.
- 23 M. S. Nashner, D. M. Somerville, P. D. Lane, D. L. Adler, J. R. Shapley and R. G. Nuzzo, *J. Am. Chem. Soc.*, 1996, **118**, 12964.
- 24 H. Song, R. M. Rioux, J. D. Hoefelmeyer, R. Komor, K. Niesz, M. Grass, P. D. Yang and G. A. Somorjai, *J. Am. Chem. Soc.*, 2006, **128**, 3027.
- 25 B. -W. Lu and K. Kawamoto, *RSC Adv.*, 2012, **2**, 6800.
- 26 D. Zhao, J. Feng, Q. Huo, N. Melosh, G. H. Fredrickson, B. F. Chmelka and G. D. Stucky, *Science*, 1998, **279**, 548.
- 27 D. Zhao, Q. Huo, J. Feng, B. F. Chmelka and G. D. Stucky, *J. Am. Chem. Soc.*, 1998, **120**, 6024.
- 28 A. L. Patterson, *Phys. Rev.*, 1939, **56**, 978.
- 29 S. J. Gregg and K. S. W. Sing, *Adsorption Surface Area and Porosity*, Academic Press, New York, 1982.
- 30 M. -Y. Cheng, C. -J. Pan and B. J. Hwang, *J. Mater. Chem.*, 2009, **19**, 5193.
- 31 L. Vradman, M. V. Landau, D. Kantorovich, Y. Koltypin and A. Gedanken, *Micropor. Mesopor. Mater.*, 2005, **79**, 307.
- 32 T. M. Eggenhuisen, J. P. den Breejen, D. Verdoes, P. E. de Jongh and de K. P. Jong, *J. Am. Chem. Soc.*, 2010, **132**, 18318.
- 33 B. -W. Lu and K. Kawamoto, *Fuel*, 2013, **103**, 699.
- 34 B. -W. Lu and K. Kawamoto, *Mater. Res. Bull.*, 2012, **47**, 1301.
- 35 B. -W. Lu, Y. Inagi and A. Endo, *J. Nanosci. Nanotechnol.*, 2011, **11**, 2361.
- 36 A. Ungureanu, B. Dragoi, A. Chiriac, S. Royer, D. Duprez and E. Dumitriu, *J. Mater. Chem.*, 2011, **21**, 12529.
- 37 P. G. Jessop, F. Joo and C. -C. Tai, *Coord. Chem. Rev.*, 2004, **248**, 2425.
- 38 T. Sakakura, J. -C. Choi and H. Yasuda, *Chem. Rev.*, 2007, **107**, 2365.
- 39 G. Centi and S. Perathoner, *Catal. Today*, 2009, **148**, 191.
- 40 M. Bourrez, F. Molton, S. Chardon-Noblat and A. Deronzier, *Angew. Chem. Int. Ed.*, 2011, **50**, 9903.
- 41 C. Federsel, R. Jackstell and M. Beller, *Angew. Chem. Int. Ed.*, 2010, **49**, 6254.
- 42 M. Mikkelsen, M. Jorgensen and F. C. Krebs, *Energy Environ. Sci.*, 2010, **3**, 43.
- 43 C. -S. Chen, W. -H. Cheng and S. -S. Lin, *Catal. Lett.*, 2000, **68**, 45.
- 44 C. -S. Chen, W. -H. Cheng and S. -S. Lin, *Catal. Lett.*, 2002, **83**, 121.
- 45 C. -S. Chen, W. -H. Cheng and S. -S. Lin, *Appl. Catal. A*, 2003, **238**, 55.
- 46 C. -S. Chen, W. -H. Cheng and S. -S. Lin, *Appl. Catal. A*, 2004, **257**, 97.
- 47 F. S. Stone and D. Waller, *Topics Catal.*, 2003, **22**, 305.
- 48 A. Goguet, F. C. Meunier and J. P. Breen, *J. Catal.*, 2004, **226**, 382.
- 49 A. Goguet, F. C. Meunier and D. Tibiletti, *J. Phys. Chem. B.*, 2004, **108**, 20240.
- 50 D. Tibiletti, A. Goguet, F. C. Meunier, J. P. Breen and R. Burch, *Chem. Commun.*, 2004, 1636.
- 51 L. -H. Wang, S. -X Zhang and Y. Liu, *J. Rare Earths*, 2008, **26**, 66.
- 52 C. -S. Chen, J. -H. Wu and T. -W. Lai, *J. Phys. Chem. C*, 2010, **114**, 15021.
- 53 C. -S. Chen, C. -C. Chen, C. -T. Chen and H. -M. Kao, *Chem. Commun.*, 2011, **47**, 2288.
- 54 B. -W. Lu and K. Kawamoto, *J. Environ. Chem. Eng.*, 2013, **1**, 300.
- 55 B. -W. Lu and K. Kawamoto, *Mater. Res. Bull.*, 2014, **53**, 70.
- 56 B. -W. Lu and K. Kawamoto, *Catal. Sci. Technol.*, 2014, **4**, 4313.
- 57 J. C. Matsubu, V. N. Yang and P. Christopher, *J. Am. Chem. Soc.*, 2015, **137**, 3076.

## Table of contents

**Dispersion and Distribution of Bimetallic Oxides in SBA-15, Its Enhanced Activity for Reverse Water Gas Shift Reaction**

Baowang Lu, Yiwen Ju, Takayuki Abe and Kastuya Kawamoto

Bimetallic Oxides could be well distributed on the SBA-15 surface, and exhibited high catalytic perforation for RWGS reaction.

